Geochimica et Cosmochimica Acta 415 (2026) 196–203

Contents lists available at ScienceDirect

Geochimica et Cosmochimica Acta

journal homepage: www.elsevier.com/locate/gca

First experimental determination of the $^{40}Ar(n, 2n)^{39}Ar$ reaction cross section and ^{39}Ar production in Earth's atmosphere

S. Bhattacharya [a], M. Paul [a,*], R.N. Sahoo [a], R. Purtschert [b], H.F.R. Hoffmann [c], M. Pichotta [c], K. Zuber [c], D. Bemmerer [d], T. Döring [d], R. Schwengner [d], M.L. Avila [e], E. Lopez-Saavedra [e], J.C. Dickerson [e], C. Fougères [e], J. McLain [e], R.C. Pardo [e], K.E. Rehm [e], R. Scott [e], I. Tolstukhin [e], R. Vondrasek [e], T. Bailey [f], L. Callahan [f], A.M. Clark [f], P. Collon [f], Y. Kashiv [f], A. Nelson [f], D. Robertson [f], D. Neto [g], C. Ugalde [g], M. Tessler [h], S. Vaintraub [h]

[a] The Hebrew University of Jerusalem, Jerusalem, 91904, Israel
[b] University of Bern, 3012, Bern, Switzerland
[c] Technical University Dresden, Dresden, Germany
[d] Helmholtz-Zentrum-Dresden-Rossendorf, 01328 Dresden, Germany
[e] Argonne National Laboratory, Argonne, IL, 60439, USA
[f] University of Notre Dame, Notre Dame, IN, 46556, USA
[g] University of Illinois Chicago, Chicago, IL, 60607, USA
[h] Soreq Nuclear Research Center, Yavne, 81800, Israel

ARTICLE INFO

Associate editor: Fred Jourdan

Dataset link: https://doi.org/10.5281/zenodo.15974057

Keywords:
$^{40}Ar(n,2n)^{39}Ar$ reaction
^{39}Ar atmospheric production
Accelerator mass spectrometry
Low-level counting

ABSTRACT

The cosmogenic $^{39}Ar(t_{1/2}$ = 268 years) isotope of argon is used for geophysical dating and tracing of underground and ocean water, as well as ice owing to its appropriate half-life and chemical inertness as a noble gas; ^{39}Ar serves also in nuclear weapon test monitoring. We measured for the first time the total cross section of the main ^{39}Ar cosmogenic production reaction in the atmosphere, namely $^{40}Ar(n, 2n)^{39}Ar$, using 14.8 ± 0.3 MeV neutrons. The neutrons, produced by a deuterium-tritium generator, impinged on a stainless steel sphere filled with Ar gas highly enriched in the ^{40}Ar isotope and were monitored by a stack of fast-neutron activation foils. The reaction yield was measured by atom counting of long-lived ^{39}Ar with noble gas accelerator mass spectrometry and, independently, by decay counting relative to atmospheric argon ($^{39}Ar/Ar = 8.12\times10^{-16}$). A total $^{40}Ar(n, 2n)^{39}Ar$ cross section of 610 ± 100 mb was determined at 14.8 ± 0.3 MeV incident neutron energy. This result serves as a benchmark for recent theoretical calculations and evaluations, found to reproduce well the experimental total cross section. We use these energy-dependent theoretical cross sections together with experimental spectra of cosmogenic neutrons at different altitudes to calculate the global average rate of neutron-induced ^{39}Ar atmospheric production, resulting in 770 ± 240 ^{39}Ar atoms/cm^2/day. The secular equilibrium between the ^{39}Ar calculated production rate and radioactive decay rate leads to a partial isotopic abundance $^{39}Ar/Ar = (5.9 \pm 1.8) \times 10^{-16}$, showing that ≈73% of atmospheric ^{39}Ar is produced by cosmogenic neutrons, the remaining part believed to be induced by muons and high-energy γ rays. The $^{40}Ar(n, 2n)^{39}Ar$ cross section at 14 MeV is also a key parameter for quantifying the anthropogenic contribution to atmospheric ^{39}Ar produced during the thermonuclear tests of the 1960s. We estimate that anthropogenic ^{39}Ar accounts for roughly 20% of the present atmospheric inventory.

1. Introduction

The radioactive ^{39}Ar nuclide with a half-life of 268 years (Stoenner et al., 1965; Golovko, 2023) occurs in nature owing to continuous production in the atmosphere by cosmic ray bombardment and in the lithosphere by both cosmogenic and radiogenic processes. It is also artificially produced in nuclear explosion tests. Owing to its half-life and chemical inertness, the radioactive ^{39}Ar nuclide is widely used in geophysical (hydrological dating) and environmental (nuclear forensics) research. Saldanha et al. (2019) have reviewed the sea-level ^{39}Ar atmospheric production modes among which the dominant reaction is $^{40}Ar(n, 2n)^{39}Ar$, together with a weaker $^{40}Ar(n, pn)^{39}Cl(t_{1/2}$ =

* Corresponding author.
E-mail address: paul@vms.huji.ac.il (M. Paul).

https://doi.org/10.1016/j.gca.2025.12.041
Received 16 July 2025; Accepted 17 December 2025
Available online 18 December 2025

Table 1
Theoretical (theo), evaluated (eval) and experimental (exp) values of the ^{40}Ar(n,2n)^{39}Ar reaction cross section (σ). Theoretical and evaluated values are calculated at 15 MeV. Experimental values are measured at the specified energy. Uncertainties of experimental values (in parenthesis) correspond to one sigma. Note that the two experimental values of MacMullin et al. (2012) correspond to two different neutron energies given in the footnotes.

	theo/eval/exp	σ (mb)	ref
ACTIVIA[a] (2008)	theo	10.1	Back and Ramachers (2008)
INCL++(ABLA 07) (2014)	theo	438[b]	Mancusi et al. (2014)
TALYS-2.00 (2023)	theo	649	Koning et al. (2023)
ENDF/B-VIII.1 (2024)	eval	667	Nobre et al. (2024)
ENDF/B-VII.1 (2011)	eval	900	Chadwick et al. (2011)
JENDL-5 (2021)	eval	900	Iwamoto et al. (2023)
MacMullin et al. (2012)[c]	exp	80(20)[d]	MacMullin et al. (2012)
"	exp	130(20)[e]	MacMullin et al. (2012)
This work[f]	exp	610 (100)	

[a] Based on Silberberg and Tsao (1973a,b).
[b] Extracted from Saldanha et al. (2019).
[c] Partial cross section to E_x(^{39}Ar)= 1267 keV.
[d] E_n = 13.4(8) MeV.
[e] E_n = 15.0(9) MeV.
[f] Total cross section for neutron energy 14.8(3) MeV.

56 min) component which feeds ^{39}Ar via β decay. The ^{40}Ar$(n,2n)^{39}$Ar reaction, with a neutron energy threshold of 10.12 MeV, occurs mainly in the upper atmosphere from the interaction of fast secondary cosmic neutrons with the stable isotope ^{40}Ar of argon (atmospheric ^{40}Ar isotopic abundance of 99.6%). Lithospheric production involves reactions induced by atmospheric and radiogenic neutrons as well as muogenic processes (see Musy and Purtschert (2023) for a recent review).

The total cross section of the ^{40}Ar$(n,2n)^{39}$Ar fast-neutron reaction has not been heretofore measured and is the object of this article in which it is determined experimentally at a neutron energy of 14.8 ± 0.3 MeV. Partial cross sections, populating two low-lying ^{39}Ar* excited states were measured in MacMullin et al. (2012) by neutron activation and γ-spectrometry. Saldanha et al. (2019) measured the ^{40}Ar$(n,2n)^{39}$Ar production yield for a neutron spectrum mimicking that of sea-level cosmogenic neutrons. Theoretical cross-section values from different models at 15 MeV are listed in Table 1, together with the experimental results from Saldanha et al. (2019) and from this work. At higher altitudes the neutron spectra are shifted towards higher neutron energies for which cross section data have so far been largely unavailable. They can be inferred from recent theoretical models, based on the fair agreement with our experimental value at 15 MeV. Validating the theoretical cross-section calculations will allow also for a more precise reconstruction of the historical ^{39}Ar input function (Cennini et al., 1995; Gu et al., 2021; Loosli and Oeschger, 1968), which is crucial for using this isotope in different dating applications in the hydro and cryosphere (Alvarado et al., 2007; Yokochi et al., 2012). Dating of air trapped in shallow ice, for example in blue-ice regions (Buizert et al., 2014) or high altitude glaciers (Hou et al., 2025), could be biased by cosmogenic ^{39}Ar *in-situ* production on various target elements, including Ar trapped in air bubbles. Our experimental value of the ^{40}Ar$(n,2n)^{39}$Ar reaction cross section plays also an essential role in the quantitative estimate of the anthropogenic ^{39}Ar input to the environment during the thermonuclear atmospheric tests releasing 14.1 MeV neutrons from deuterium-tritium fusion (Loosli and Oeschger, 1968; Gu et al., 2021). Experimental knowledge of the relevant $(n,2n)$ reaction will allow a more reliable assessment of this contribution to the ^{39}Ar atmospheric inventory.

An independent incentive for the present measurement came from an experiment using laser-induced inertial confinement fusion performed at National Ignition Facility (see a review in Cerjan et al. (2018)). In this experiment Ar seeds were added to a deuterium-tritium (DT) capsule to study neutron-induced reactions in a high-density and high neutron density plasma produced during implosion. The ^{40}Ar$(n,2n)^{39}$Ar reaction serves there as an internal monitor of the 14 MeV neutrons produced by DT fusion.

Section 2 describes our experimental method based on 14.8 MeV neutron activation of ^{40}Ar and two independent methods of detection of ^{39}Ar, namely atom counting by noble gas accelerator mass spectrometry (NOGAMS) and low-level counting (LLC) of its decay β's. Section 3 presents our cross section results and these results are discussed in Section 4 in the context of ^{39}Ar cosmogenic and anthropogenic atmospheric production.

2. Materials and methods

2.1. Sample preparation and neutron activation

Argon samples enriched in ^{40}Ar were prepared for activation at Helmholtz Zentrum Dresden-Rossendorf (HZDR) by filling cryogenically two spheres, denoted as HZDR and HZDR23. The spheres (Fig. 1a), made of stainless steel, are 20 mm in inner diameter with 0.6 mm wall thickness and sealed by a 3 mm diameter spring loaded ball that can be released by a set screw to transfer the gas to a secondary container after irradiation. Table 2 lists the properties of the samples.

The HZDR and HZDR23 spheres were separately activated in 2021 and 2023, respectively, by neutrons from the D-T neutron generator (Klix et al., 2018) of Technical University Dresden (TUD). The neutrons were generated by a 300 keV deuteron beam bombarding a planar tritium thick target of titanium hydride with a diameter of 1 cm. The spheres (Fig. 1b), sandwiched between activation monitors appropriate for fast neutrons (Nb, Zr and Al foils of 20 mm diameter) were positioned as Nb-Zr-Al-sphere-Al-Zr-Nb in the forward direction 10 cm from the accelerator beam stop holding the tritium target. The Zr monitors, used to determine the effective energy of the neutron beam via the energy-dependent ^{90}Zr$(n,2n)^{89}$Zr cross section (Nobre et al., 2024), yielded values of 14.67 ± 0.15 MeV and 15.0 ± 0.4 MeV for the 2021 and 2023 campaigns, respectively. We adopt the unweighted average 14.8 ± 0.3 MeV of the experimental values as representative of both experiments. The value is also consistent with that of the mean and standard deviation calculated from the experimental excitation function of the $t(d,n)^4$He reaction (Davidenko et al., 1957) between the deuteron bombarding energy of 300 keV and zero for the thick target used in our experiment. The irradiation duration per campaign was 5 h (including an interruption of 1 h for the HZDR23 sample). The neutron field intensity varied over time by ≈ 30% as measured by the deuteron beam intensity on target. The time profile and decay corrections were later taken into account in the analysis. After each activation, the activity of the monitor samples was measured using a lead-shielded germanium detector with a distance of 5 cm (10 cm) between crystal and sample in the 2021 (2023) experiments. The germanium detector's full energy efficiency was calibrated using point-shaped reference sources.

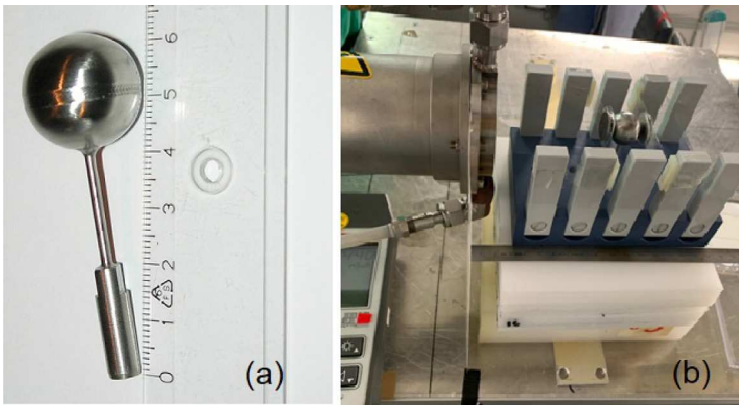

Fig. 1. Photograph of (a) ^{40}Ar-filled sphere used for activation at the TUD DT neutron generator; (b) activation setup (from left to right): accelerator beam pipe ending with the beam stop holding the tritium target, two rows of (light gray) rectangular neutron absorbers, the 20 mm diameter sphere sandwiched between Al, Zr and Nb monitor foils of same diameter. The sphere is positioned at 10 cm from the beam stop holding the tritium target.

Table 2
Activated Ar samples. Uncertainties in fluence values correspond to one sigma.

	SNRC quartz ampoule	HZDR stainless steel sphere	HZDR23 stainless steel sphere
^{40}Ar (%)	0.006	99.992	99.992
^{38}Ar (%)	99.961	0.004	0.004
^{36}Ar (%)	0.033	0.004	0.004
Ar mass (g)	0.0053	0.3903	1.0176
neutron fluence (cm^{-2})	$\approx 2\times10^{14}$ [a]	$6.92(24)\times10^{11}$ [b]	$7.74(56)\times10^{11}$ [b]

[a] Thermal neutron activation at SNRC. Sample SNRC was diluted after activation with ^{38}Ar(99.96%) and ^{nat}Ar to a final isotopic ratio of ^{38}Ar/^{40}Ar$\approx$ 9.5% for the NOGAMS setup and ^{38,40}Ar transmission measurements; see 2.2.1.
[b] 14.8 ± 0.3 MeV neutron activation at the TUD neutron generator.

Correction factors for geometry and γ self absorption in the monitor foils were obtained from detailed GEANT4 simulations (Agostinelli et al., 2003). The integral neutron fluences (see Table 2) were determined by the Nb (0.7242 g/cm^2) and Al (0.2303 g/cm^2) monitors. The cross section of the ^{93}Nb$(n,2n)^{92m}$Nb(10.15 d) reaction (0.466 ± 0.019) b (Kostal et al., 2023) and of the ^{27}Al$(n,\alpha)^{24}$Na(14.96 hr) reaction (0.1216 ± 0.0051) b (W. Mannhart, 2007) were used. These experimental cross sections and their uncertainties represent well the spread of available evaluated cross sections at our effective neutron energy. For each of the Nb and Al sample pairs, the geometric mean of both fluence values describes the fluence in their center assuming exponential neutron attenuation. The fluences extracted from the Al and Nb monitors are consistent and were combined as a weighted mean and its variance (Table 2). The one-sigma systematic uncertainty (2.0%) of the full energy efficiency is determined conservatively as the maximum uncertainty of the calibration sources' absolute activity. Uncertainties in monitor mass (< 1%), literature half-lives contribution (0.2%) and counting statistics (0.2%) are taken into account.

After appropriate radioactive cooling, each sphere was shipped to Argonne National Laboratory (ANL) and its argon content was separated in two aliquots, one to be analyzed for its ^{39}Ar/^{40}Ar isotopic ratio by NOGAMS at ANL and the second for its β activity by LLC at University of Bern.

In addition, an Ar sample highly enriched in ^{38}Ar contained in a small quartz ampoule (Table 2) was activated at the Soreq Nuclear Research Center (SNRC) with thermal neutrons from a 5 MW reactor to produce ^{39}Ar by ^{38}Ar$(n,\gamma)^{39}$Ar. After activation, the SNRC sample was diluted with ^{38}Ar and ^{nat}Ar to obtain a sample volume and isotopic abundance appropriate for establishing the NOGAMS and LLC ^{39}Ar detection conditions and to measure the accelerator transmission efficiencies for ^{38}Ar and ^{40}Ar (see Section 2.2.1).

2.2. ^{39}Ar detection

2.2.1. NOGAMS analysis

Noble gas accelerator mass spectrometry, an offshoot of standard accelerator mass spectrometry (AMS) (Kutschera et al., 2023), is an atom counting technique based on positive ion injection, enabling ultrasensitive detection of noble gas isotopes; the latter do not form stable negative ions used in standard AMS and are excluded thereof. The technique was developed at Argonne National Laboratory (ANL) for the detection of ^{39}Ar and geophysical dating (Collon et al., 2004) and has been applied since to nuclear astrophysics (Tessler et al., 2018; Nassar et al., 2005); see Paul et al. (2019) for a detailed description. Fig. 2(a) shows a schematic illustration of the facility at the ATLAS accelerator at ANL. The activated gas samples (Table 2) are loaded into the ECR3 Electron Cyclotron Resonance ion source and highly charged Ar^{8+} ions are extracted. Following mass-to-charge (m/q) magnetic analysis, ^{38,39,40}Ar ions are sequentially injected and accelerated by the ATLAS superconducting linear accelerator, which acts as an additional m/q filter, to an energy of 5.3 MeV/nucleon. The stable ^{38,40}Ar^{8+} charge current (of the order of nA) is measured in an electron-suppressed Faraday cup; quantitative attenuation of the more intense ^{40}Ar^{8+} current is applied (see Table 3). ^{39}Ar and parasitic ions (isobaric ions and ions with close-by m/q ratio transported by the accelerator), with rates of 1–100 s^{-1} in our experiments, are analyzed by the gas-filled Enge spectrograph (Paul et al., 1989). The ions are spatially separated therein as function of their ratio of mass to mean ionic charge ($m/\bar{q}$); the latter results from atomic collisions which change the ionic charge in the gas-filled magnet. Owing to their energy of a few MeV/nucleon, the ions are further identified by energy loss measurements in the Monica position-sensitive multi-anode ionization chamber (Callahan et al., 2022). Dispersion (spatial separation) along the focal plane is measured by the parameter $P23 = (A3-A2)/(A3+A2)$ where Ai denotes here the energy loss signal in the corresponding anode (Fig. 2(b)).

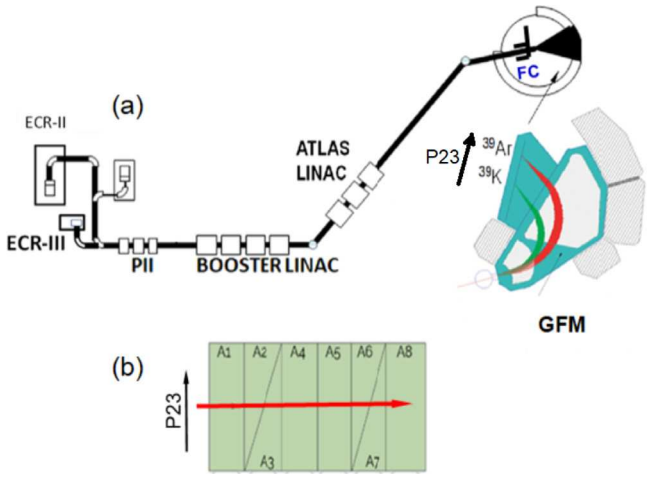

Fig. 2. Schematic diagram of: (a) the Noble Gas Accelerator Mass Spectrometry setup at Argonne National Laboratory for ^{39}Ar detection. $^{38,39,40}Ar^{8+}$ ions are sequentially injected from the Electron Cyclotron Resonance (ECR-III) ion source and accelerated through the Positive Ion Injector (PII) and Booster- and ATLAS-Linac. Intensity of stable isotope $^{38,40}Ar^{8+}$ accelerated beams are measured as charge current (typically of the order of nA) in an electron-suppressed Faraday Cup (FC). The rare isotope ^{39}Ar is counted as individual ions in the Enge Gas-Filled Magnetic spectrograph (GFM); (b) the multi-anode plate of the Monica ionization chamber (Callahan et al., 2022) located perpendicular to the focal plane of the GFM. Energy loss signals for ions entering the detector are extracted from each anode A1-A8 for identification. The position P23 along the GFM dispersion axis is measured by the normalized difference of signals in the split anodes A2 and A3 (P23 = (A3−A2)/A3+A2)).

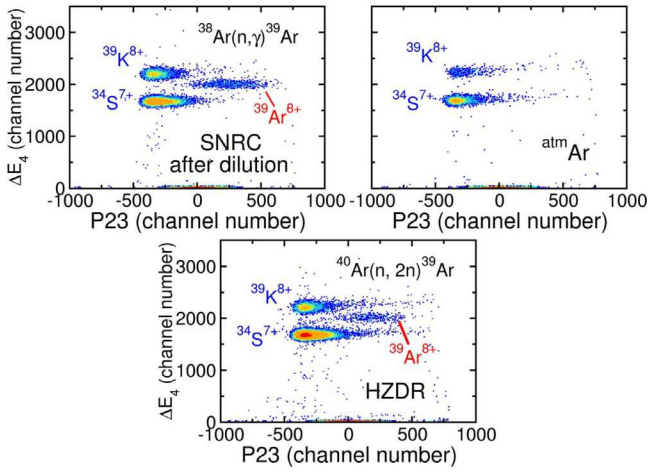

Fig. 3. Identification spectrum of ^{39}Ar ions in the detector measured for: (top left) the diluted SNRC sample irradiated at Soreq NRC; (top right) a non-irradiated atmospheric Ar sample (^{39}Ar/Ar = 8.12×10^{-16}) where ^{39}Ar is below detection sensitivity; (bottom) the HZDR (2022) irradiated sample. The horizontal axis represents the dispersion along the focal plane and the vertical axis represents the differential energy loss signal measured in the fourth anode of the focal-plane ionization chamber. The upper and lower left-hand groups originate from $^{39}K^{8+}$ (stable isobar of ^{39}Ar) and $^{34}S^{7+}$ ions, respectively, both chemical impurities in the ion source. $^{34}S^{7+}$ ions are nearly degenerate in m/q with $^{39}Ar^{8+}$.

Fig. 3 displays an example of identification spectra where the group of ^{39}Ar ions, clearly separated from isobaric ^{39}K ions and parasitic ^{34}S ions (originating from chemical impurity in the ion source), can be counted. A similar spectrum accumulated when a ^{nat}Ar sample was loaded in the ion source shows a negligible background in the region

Table 3
^{39}Ar/Ar isotopic abundance and ^{40}Ar$(n, 2n)^{39}$Ar extracted cross section value for irradiated HZDR and HZDR23 samples in NOGAMS and LLC measurements. Final values were rounded to relevant number of digits. Uncertainties (in parenthesis) correspond to one sigma.

	HZDR		HZDR23
	2021	2022	2023
NOGAMS			
Ave. FC $^{40}Ar^{8+}$ (nA)	1.8(1)	1.75(3)	2.6(1)
$^{40}Ar^{8+}$ attenuation factor	26.7(8)	26.8(8)	28.0(8)
Ave. ^{39}Ar rate-gross (cpm)	0.96(5)	0.92(4)	1.56(7)
Ave. ^{39}Ar rate-net (cpm)	0.70(4)	0.89(4)	1.50(7)
^{39}Ar fractionation correction	1.13(10)	1.08(11)	1.03(5)
R_{net}[a] (10^{-13}) - NOGAMS	3.5(3)	4.4(5)	4.6(4)
cross section (mb)- NOGAMS	510(50)	640(80)	590(70)
LLC			
sample count rate-gross (cpm)		0.455(5)	0.532(9)
sample count rate-net (cpm)		0.319(6)	0.409(9)
atmosphere-net (cpm)		0.059(9)	0.058(6)
R_{net}[a](sample)/R_{net}[a](atmosphere)		460(70)	727(60)
R_{net}[a](count. gas)/R_{net}[a](atmosphere)		5.5(8)	7.1(7)
R_{net}[a] (10^{-13}) - LLC		3.7(6)	5.9(4)
cross section (mb) - LLC		540(90)	760(80)
grand average cross section (mb)		610(100)	

[a] Background subtracted ^{39}Ar/Ar isotopic abundance.

of ^{39}Ar interest, consistent with the atmospheric ^{39}Ar cosmogenic abundance (^{39}Ar/Ar= 8.12×10^{-16} (Loosli, 1983; Benetti et al., 2007; Golovko, 2023)) below the sensitivity of the present measurements.

The (absolute) ^{39}Ar/^{40}Ar isotopic abundance measured by NOGAMS in each of the experiments (2021, 2022, 2023) listed in Table 3 is determined by the ratio of the ^{39}Ar count rate (s^{-1}) measured in the Monica detector and the $^{40}Ar^{8+}$ ion rate $i/8e$, where i is the charge current in A measured in the Faraday cup and e is the electron charge in C, respectively. The charge current i is corrected for the beam attenuation factor. An additional fractionation correction (see Table 3) is applied to take into account the ratio of ^{39}Ar and ^{40}Ar accelerator transmission efficiencies. The ^{39}Ar transmission efficiency is determined in each experiment by the average transmission efficiency for ^{38}Ar and ^{40}Ar using the diluted SNRC sample; the latter (of the order of 50%) are themselves measured as ratio of charge currents after the ion source and at the magnetic spectrograph entrance. The ion transmission efficiency between the Faraday cup and the Monica detector was established to be 100%.

2.2.2. Low-level counting analysis

A fraction of the irradiated ^{40}Ar gas was transferred into stainless steel containers and shipped to the University of Bern. The gas volume (6.75 cm^3) was determined and subsequently diluted by a factor of 120 using bottled argon extracted from the atmosphere in 2018. 6% of methane was added as a quenching gas (Riedmann and Purtschert, 2016). The ^{39}Ar activity was measured in a 100 cc proportional counter operated at a pressure of 6500 mb. The LLC laboratory is located 35 m underground, reducing the muon flux by a factor of 10. The β energy deposited from ^{39}Ar decays is recorded using a 7-bit Multi-Channel Analyzer (MCA). The detector background is determined through separate runs with argon depleted in ^{39}Ar by a factor of 20–50, sourced from underground (Xu et al., 2015). Three measurements are performed to assess the ^{39}Ar content of the sample: one using the depleted argon to quantify background, one with atmospheric argon as a reference, and one with the sample itself. The ^{39}Ar activity of the sample is obtained by subtracting the measured background from the total activity and then comparing to the background-subtracted activity of atmospheric argon. Dilution corrected results (Table 3) are reported as the ^{39}Ar/Ar ratio relative to the atmospheric reference value of 8.12×10^{-16}.

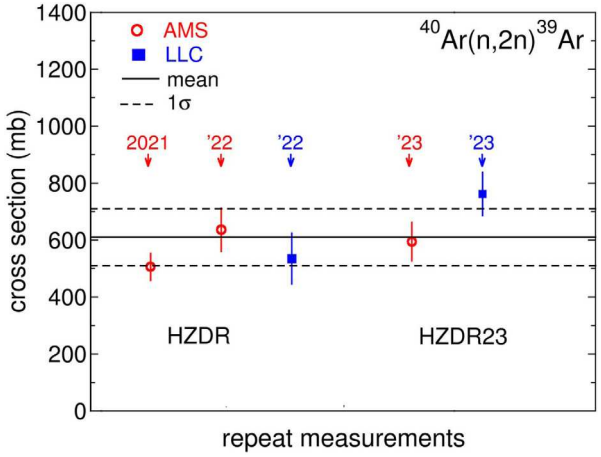

Fig. 4. Cross section of the $^{40}\mathrm{Ar}(n,2n)^{39}\mathrm{Ar}$ reaction measured by AMS (open symbols) and LLC (solid symbols). The error bars represent 1σ uncertainty derived from repeat measurements in each experiment. The adopted unweighted mean and standard deviation (dashed lines) of the measured cross section values are shown.

Table 4
Table of uncertainties (one sigma) for HZDR23 measurements.

Source of uncertainty	Uncertainty (%)
Ave. FC $^{40}Ar^{8+}$	3.8
Stable beam attenuation	3.0
Ave. ^{39}Ar rate-net	4.7
^{39}Ar fractionation correction	4.9
^{39}Ar/^{40}Ar - NOGAMS	8.3
neutron fluence	7.2
cross sect. - NOGAMS	11.0
count rate-net	2.2
atm-net	10.3
R/Ratm-counting gas	9.8
R/Ratm-sample	8.2
^{39}Ar/^{40}Ar - LLC	6.8
cross sect. - LLC	10.0
atmospheric neutron flux spectrum	24[a]
lat., long., solar act.,	20[b]
overall uncertainty	31

[a] Maximum uncertainty quoted for measured neutron spectrum (Goldhagen, 2000).
[b] (Slayman, 2011).

3. Results

The cross section σ_{39} of the $^{40}\mathrm{Ar}(n,2n)^{39}\mathrm{Ar}$ reaction is extracted from the measured ^{39}Ar/^{40}Ar isotopic ratios of Table 3 using the expression $^{39}\mathrm{Ar}/^{40}\mathrm{Ar} = \Phi \cdot t \cdot \sigma_{39}$, where $\Phi \cdot t$ denotes the 14.8 MeV neutron fluence (Table 2). The contribution of the $^{40}\mathrm{Ar}(n,pn)^{39}\mathrm{Cl}$ reaction to the feeding of ^{39}Ar, the cross section of which was measured to be 1.7(2) mb (Husain and Kuroda, 1968), is negligible. The unweighted mean and standard deviation of all our measured values of the $^{40}\mathrm{Ar}(n,2n)^{39}\mathrm{Ar}$ reaction cross section (Fig. 4 and Table 3) are 610 ± 100 mb at 14.8 ± 0.3 MeV. Table 4 lists the overall uncertainties for the sample HZDR23.

4. Discussion

4.1. Cosmogenic production of ^{39}Ar in the atmosphere

We note in Table 1 that values calculated by the recent version (2.00) the theoretical TALYS code (Koning et al., 2023) and that of the ENDF/B-VIII.1 evaluation (Nobre et al., 2024) are in good agreement with our experimental value of the $^{40}\mathrm{Ar}(n,2n)^{39}\mathrm{Ar}$ reaction

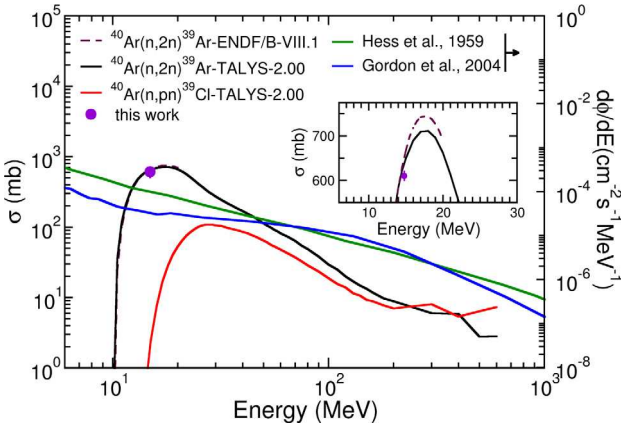

Fig. 5. Cross section (left axis) of the $^{40}\mathrm{Ar}(n,2n)^{39}\mathrm{Ar}$ and $^{40}\mathrm{Ar}(n,pn)^{39}\mathrm{Cl}$ reactions calculated by the ENDF/B-VIII.1 evaluation and the TALYS-2.00 code as a function of neutron energy. Our experimental value and the 1σ uncertainty for the $^{40}\mathrm{Ar}(n,2n)^{39}\mathrm{Ar}$ cross section at 14.8 MeV is plotted. The insert shows the region around the experimental point in linear scale. Experimental spectra (right axis) of neutron flux of cosmic origin at sea-level are also plotted.

Table 5
^{39}Ar production rate P at different altitudes, calculated with Eq. (1).
Source: Based on cosmic flux spectra from Goldhagen et al. (2003), Gordon et al. (2004), Hess et al. (1959).

Altitude (km)	P (10^3 atoms/kg$_{Ar}$/day)	Based on
0.2	0.744	Gordon et al. (2004)
11.9	192	Goldhagen et al. (2003)
16.2	474	
20.0	530	
0	1.47	Hess et al. (1959)
3.2	112	
12.2	237	

cross section; see also Fig. 5 which shows the energy dependence of the theoretical TALYS-2.00 cross section (Koning et al., 2023) of the $^{40}\mathrm{Ar}(n,2n)^{39}\mathrm{Ar}$ and $^{40}\mathrm{Ar}(n,pn)^{39}\mathrm{Cl}$ reactions. The production yield via the (n,pn) reaction, negligible in our experiment at 14.8 MeV, amounts to ≈ 20% of the $(n,2n)$ reaction over the whole energy range. The good agreement of the theoretical TALYS-2.00 value of the $^{40}\mathrm{Ar}(n,2n)^{39}\mathrm{Ar}$ cross section with the experimental value at 14.8 MeV obtained in this work gives us confidence in using TALYS values to calculate the atmospheric production rate of ^{39}Ar at different altitudes from cosmogenic neutrons, using experimental neutron spectra (Hess et al., 1959; Goldhagen et al., 2003; Gordon et al., 2004); Fig. 5 illustrates such spectra at sea level. The ^{39}Ar production rate $P(z)$ (atoms/kg$_{Ar}$/day) at altitude z from the interaction of cosmic ray neutrons can be written as,

$$P(z) = N_{Ar} \cdot n_{s/day} \int \frac{d\phi(E,z)}{dE}\sigma(E)\, dE, \qquad (1)$$

where N_{Ar} is the number of Ar atoms per kg of argon, $n_{s/day} = 86400$ the number of seconds in a day, z the altitude (cm), $d\phi(E,z)/dE$ is the cosmic-ray induced neutron flux spectrum (neutrons/cm^2/s/MeV) and $\sigma(E) = \sigma_{(n,2n)}(E) + \sigma_{(n,pn)}(E)$ is the sum of the $^{40}\mathrm{Ar}(n,2n)$ and $^{40}\mathrm{Ar}(n,pn)$ cross sections (cm^2) calculated using the TALYS-2.00 code. Note that we use in this section the symbol Ar to denote either elemental Ar or ^{40}Ar. The values of $P(z)$ are given in Table 5 and shown in Fig. 6(a). The production rates, shown in Table 5, confirm the expected overwhelming contribution of ^{39}Ar production at high altitudes compared to the sea-level value. In Fig. 6, we also average the $P(z)$ values extracted from the flux data of Hess et al. (1959), Gordon et al. (2004), Goldhagen et al. (2003) taken at different locations and times using the latitude, longitude and solar activity dependence of the neutron flux presented

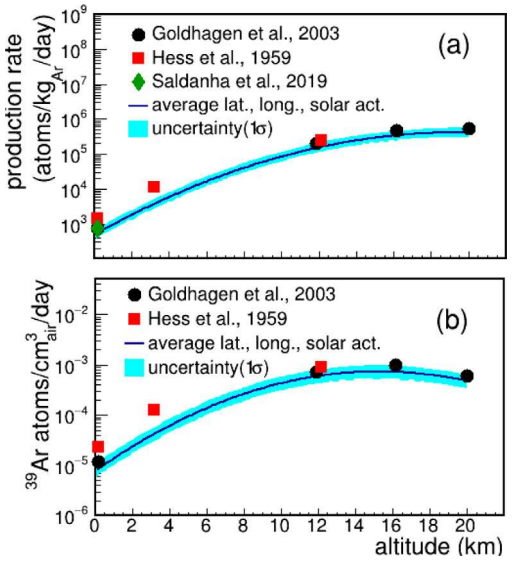

Fig. 6. (a) Cosmogenic atmospheric production rate of ^{39}Ar at different altitudes calculated using energy-dependent cross sections of the TALYS-2.00 code (benchmarked by our experimental value of ^{40}Ar$(n,2n)^{39}$Ar reaction cross section at 14.8 MeV, see Fig. 5) and spectra of cosmic-ray induced neutrons at different altitudes from Hess et al. (1959), Goldhagen et al. (2003), Gordon et al. (2004) (solid symbols). The data are summed production rates via the ^{40}Ar$(n,2n)^{39}$Ar and ^{40}Ar$(n,pn)^{39}$Cl reactions. Our calculated value for sea-level production rate is in good agreement with the experimental value of Saldanha et al. (2019) obtained with an artificial neutron flux spectrum. The solid line represents a fit ($\bar{P}(z)$ in the text) of the production rates at the discrete locations and altitudes after averaging for dependence on latitude, longitude, and solar activity (Woolf et al., 2019) (see text); the blue band denotes a 1σ uncertainty partially based on Goldhagen et al. (2003). (b) Production of ^{39}Ar atoms per cm^3 of air per day at different altitudes (solid symbols), calculated using the production rates in (a). The solid line (blue band) is calculated using the averaged production rate (1σ uncertainty) of (a).

in Woolf et al. (2019). This averaging, which we denote below by $\bar{P}(z)$, is justified by the short time scales (1–10 yr) of atmospheric exchanges (Hobbs, 2000) and solar activity (11 yr), compared to the ^{39}Ar half-life (268 yr) and leads to consider the ^{39}Ar abundance as homogeneous in the atmosphere.

We note that the value determined here of 744 ^{39}Ar atoms/kg$_{Ar}$/day for sea-level production rate is consistent with the experimental value (759 ± 128 ^{39}Ar atoms/kg$_{Ar}$/day) of Saldanha et al. (2019) who used an artificial neutron spectrum and scaled their values using different theoretical models. We show also in Fig. 6(b) the ^{39}Ar production rates per cm^3 of air at different altitudes where the increased rates shown in Fig. 6(a) are mitigated at high altitudes by the lower air density.

Using the averaged altitude-dependent ^{39}Ar production rate $\bar{P}(z)$ (atoms/kg$_{Ar}$/day), we can express the total ^{39}Ar production rate $\bar{P}_{^{39}Ar}$ in an air column of with a cross-sectional area of 1 cm^2 cross section as

$$\frac{d\,\bar{P}_{^{39}Ar}}{dS} = \int_{sea\ level}^{H_{max}} \bar{P}(z)\ m_f\ \rho_{air}(z)\ dz, \tag{2}$$

where m_f is the mass fraction of argon in air, and $\rho_{air}(z)$ is the air density (in kg/cm^3) at altitude z(cm), calculated from United States Committee on Extension to the Standard Atmosphere (1976). The total production rate, calculated from sea level up to an altitude of 20 km (denoted as H_{max}), is found to be 770 ± 240 ^{39}Ar atoms/cm^2/day.

We can now calculate the ^{39}Ar content of the whole air column and its ^{39}Ar/Ar isotopic ratio at secular equilibrium between cosmogenic production and radioactive decay. Implicit in this calculation is the negligible effect of chemical or physical sinks via chemical binding, adsorption, or dissolution (Ozima and Podosek, 2004). The steady-state ^{39}Ar/Ar ratio is expressed as:

$$^{39}Ar/Ar\ = \frac{(d\,\bar{P}_{^{39}Ar}/dS)/\lambda}{dn_{Ar}/dS}, \tag{3}$$

where λ is the decay constant of ^{39}Ar in day^{-1} and dn_{Ar}/dS denotes the number of Ar atoms per cm^2 of air column, calculated using the following relation:

$$dn_{Ar}/dS = \int_{sea\ level}^{H_{max}} \frac{N_A\ m_f\ \rho_{air}(z)}{M_{Ar}}\ dz. \tag{4}$$

Here, N_A denotes Avogadro's constant and M_{Ar} is the molar mass of argon (in kg). Based on the experimental neutron flux spectra $d\phi(E,z)/dE$ from Goldhagen et al. (2003), and using the ^{39}Ar production rate calculated with Eq. (2), the steady state ^{39}Ar/Ar ratio from neutron-induced production in the atmosphere up to an altitude of 20 km is $(5.9 \pm 1.8)\times10^{-16}$. The contribution of the ^{40}Ar$(n,pn)^{39}$Cl is $\approx 20\%$ of this value. Comparison with the experimental value of ^{39}Ar/Ar$=(8.12 \pm 0.30)\times10^{-16}$ in the atmosphere (Loosli, 1983; Benetti et al., 2007; Golovko, 2023) indicates that 73% of ^{39}Ar is produced by cosmic-ray induced neutrons. This fraction is consistent with the estimate (72.3%) of Saldanha et al. (2019) based on sea-level production only. We note in this context that ^{39}Ar production in shallow soils, dominated by the ^{39}K$(n,p)^{39}$Ar reaction with cosmogenic neutrons, does not contribute significantly to the atmospheric ^{39}Ar/Ar ratio (Fritz et al., 2021; Musy and Purtschert, 2023). Muon and high-energy γ rays induced reactions on ^{40}Ar are considered in Saldanha et al. (2019) to account for the major part of the remaining natural ^{39}Ar production in the atmosphere.

4.2. Anthropogenic production of ^{39}Ar in the atmosphere

The presence of an anthropogenic contribution to atmospheric ^{39}Ar, attributed to DT-neutrons from thermonuclear tests, was first noted by Loosli and Oeschger (1968). They compared the ^{39}Ar specific activity in argon samples collected in 1940 and in 1959–1967, and estimated a contribution of $\lesssim 7\%$. More recently, (Gu et al., 2021) reconstructed the atmospheric ^{39}Ar/Ar history and estimated this contribution to be $\lesssim 15\%$ of the total atmospheric ^{39}Ar inventory. The ^{40}Ar$(n,2n)^{39}$Ar reaction cross section measured in this work at 14.8 MeV and its fair agreement with recent theoretical models (see Table 1 and Section 4) are essential data for a reliable estimate of the anthropogenic contribution to atmospheric ^{39}Ar, originating mainly from the DT component of the thermonuclear devices. We calculate the ^{39}Ar production via the ^{40}Ar$(n,2n)^{39}$Ar reaction by simulating the transport of 14.1 MeV neutrons in the atmosphere using the GEANT4 code (Agostinelli et al., 2003) and the TALYS-2.00 code benchmarked in Section 4; a standard atmosphere composition is taken from United States Committee on Extension to the Standard Atmosphere (1976). We find that a fraction of $1.5 - 3.4 \times 10^{-3}$ of emitted DT neutrons (14.1 MeV) produces ^{39}Ar via the $(n,2n)$ reaction for high- to low-altitude tests, respectively. It is remarkable that the value of 2×10^{-3} originally quoted in Loosli and Oeschger (1968) is fully consistent with this calculation. Using the neutron production of 8×10^{28} estimated by Gu et al. (2021) for all nuclear tests, our simulation yields between 1.2×10^{26} and 2.7×10^{26} anthropogenic ^{39}Ar atoms, corresponding to $\approx 20\%$ of the atmospheric cosmogenic ^{39}Ar inventory that is in qualitative agreement with the findings in Gu et al. (2021).

5. Conclusions

Using 14.8 MeV neutrons from a DT neutron generator, we have determined for the first time the total cross section of the ^{40}Ar$(n,2n)^{39}$Ar ($t_{1/2}$ = 268 yr) reaction as 610 ± 100 mb. The cross section was determined by ^{39}Ar atom counting with noble gas accelerator mass spectrometry and independently by low-level β counting relative to atmospheric argon. The recent TALYS-2.00 theoretical cross section

values of the reaction (Koning et al., 2023) and the ENDF/B-VIII.1 evaluation (Nobre et al., 2024) are found to be in good agreement with our experimental value. We used the TALYS-2.00 energy-dependent theoretical cross section of the $^{40}Ar(n,2n)^{39}Ar$ reaction, benchmarked at 14.8 MeV by our experimental value and that of the $^{40}Ar(n,pn)^{39}Cl(t_{1/2}$ = 56 min) reaction (feeding long-lived ^{39}Ar), together with experimental spectra of cosmic-ray induced neutrons, to calculate a production rate of 770 ± 240 ^{39}Ar atoms/cm^2/day in the atmosphere up to an altitude of 20 km. Comparison of the derived neutron-produced $^{39}Ar/Ar$ isotopic abundance at secular equilibrium between production and decay with the experimental $^{39}Ar/Ar$ atmospheric abundance shows that 73% of atmospheric ^{39}Ar originate in cosmic-ray induced neutrons, in agreement with an earlier result (Saldanha et al., 2019) based on sea-level production alone. This work establishes on firmer quantitative grounds the neutron-induced origin of the cosmogenic ^{39}Ar abundance in the Earth's atmosphere. We use the experimental value of the $^{40}Ar(n,2n)^{39}Ar$ reaction cross section for 14 MeV DT neutrons also to estimate the contribution of the thermonuclear tests of the 1960's to ^{39}Ar in the atmosphere; this contribution is derived to be ≈ 20% of the ^{39}Ar atmospheric inventory.

CRediT authorship contribution statement

S. Bhattacharya: Writing – review & editing, Writing – original draft, Software, Methodology, Formal analysis, Data curation. **M. Paul:** Writing – review & editing, Writing – original draft, Validation, Resources, Project administration, Methodology, Investigation, Funding acquisition, Conceptualization. **R.N. Sahoo:** Writing – review & editing, Software, Data curation. **R. Purtschert:** Writing – review & editing, Writing – original draft, Methodology, Investigation, Formal analysis, Data curation, Conceptualization. **H.F.R. Hoffmann:** Writing – review & editing, Writing – original draft, Methodology, Formal analysis, Data curation. **M. Pichotta:** Software, Formal analysis, Data curation. **K. Zuber:** Writing – review & editing, Supervision. **D. Bemmerer:** Writing – review & editing, Supervision, Resources, Formal analysis. **T. Döring:** Writing – review & editing, Resources, Data curation. **R. Schwengner:** Writing – review & editing, Validation, Resources. **M.L. Avila:** Writing – review & editing, Software, Resources. **E. Lopez-Saavedra:** Writing – review & editing, Validation, Software. **J.C. Dickerson:** Writing – review & editing, Supervision, Resources. **C. Fougères:** Writing – review & editing, Software, Formal analysis. **J. McLain:** Writing – review & editing, Resources, Investigation. **R.C. Pardo:** Writing – review & editing, Supervision, Methodology, Conceptualization. **K.E. Rehm:** Writing – review & editing, Resources, Investigation. **R. Scott:** Writing – review & editing, Resources, Investigation. **I. Tolstukhin:** Writing – review & editing, Software, Resources, Investigation. **R. Vondrasek:** Writing – review & editing, Resources, Methodology. **T. Bailey:** Writing – review & editing, Software, Data curation. **L. Callahan:** Writing – review & editing, Validation, Software, Investigation. **A.M. Clark:** Writing – review & editing, Validation, Software, Investigation. **P. Collon:** Writing – review & editing, Supervision, Resources, Investigation. **Y. Kashiv:** Writing – review & editing, Validation, Investigation, Conceptualization. **A. Nelson:** Writing – review & editing, Investigation. **D. Robertson:** Writing – review & editing, Resources, Investigation. **D. Neto:** Writing – review & editing, Software, Investigation. **C. Ugalde:** Writing – review & editing, Supervision, Investigation. **M. Tessler:** Writing – review & editing, Investigation. **S. Vaintraub:** Writing – review & editing, Investigation.

Declaration of competing interest

The authors declare that they have no known competing financial interests or personal relationships that could have appeared to influence the work reported in this paper.

Acknowledgments

We thank the ATLAS Operation staff at Argonne National Laboratory for their dedication to this experiment. We thank Rüdiger Schanda for his help with the LLC measurements in Bern. We gratefully acknowledge the support of USA-Israel Binational Science Foundation (BSF), Israel under grant BSF-2020136, Pazy Foundation (Israel) and EU program ChETEC-INFRA, 101008324, and BMFTR (05A23OD1). This material is based upon work supported by the U.S. Department of Energy, Office of Science, Office of Nuclear Physics, under Contract No. DE-AC02-06CH11357. This research used resources of Argonne National Laboratory's ATLAS facility, which is a DOE Office of Science User Facility. This work is supported in part by National Science Foundation, USA Grant No. NSF PHY-2310059.

Data availability

Data are available through Zenodo at https://doi.org/10.5281/zenodo.15974057.

References

Agostinelli, S., Allison, J., Amako, K., Apostolakis, J., Araujo, H., et al., 2003. GEANT4 - a simulation toolkit. Nucl. Instrum. Methods Phys. Res. Sect. A 506, 250–303.

Alvarado, J.A.C., Purtschert, R., Barbecot, F., Chabault, C., Rueedi, J., Schneider, V., Aeschbach-Hertig, W., Kipfer, R., Loosli, H.H., 2007. Constraining the age distribution of highly mixed groundwater using ^{39}Ar: A multiple environmental tracer ($^3H/^3He$, ^{85}Kr, ^{39}Ar, and ^{14}C) study in the semiconfined fontainebleau sands aquifer (France). Water Resour. Res. 43.

Back, J., Ramachers, Y.A., 2008. ACTIVIA: Calculation of isotope production cross-sections and yields. Nucl. Instruments Methods Phys. Res. Sect. A: Accel. Spectrometers, Detect. Assoc. Equip. 586, 286–294.

Benetti, P., Calaprice, F., Calligarich, E., Cambiaghi, M., Carbonara, F., et al., 2007. Measurement of the specific activity of ^{39}Ar in natural argon. Nucl. Instruments Methods Phys. Res. Sect. A: Accel. Spectrometers, Detect. Assoc. Equip. 574, 83–88.

Buizert, C., Baggenstos, D., Jiang, W., Purtschert, R., Petrenko, V.V., Lu, Z.T., Müller, P., Kuhl, T., Lee, J., Severinghaus, J.P., Brook, E.J., 2014. Radiometric ^{81}Kr dating identifies 120 000-year-old ice at Taylor Glacier, Antarctica. Proc. Natl. Acad. Sci. 111, 6876–6881.

Callahan, L.K., Collon, P., Paul, M., Avila, M., Back, B., et al., 2022. Initial tests of accelerator mass spectrometry with the argonne gas-filled analyzer and the commissioning of the MONICA detector. Nucl. Instruments Methods Phys. Res. Sect. B: Beam Interactions Mater. Atoms 532, 7–12.

Cennini, P., Cittolin, S., Dzialo Giudice, D., Revol, J., Rubbia, C., et al., 1995. On atmospheric ^{39}Ar and ^{42}Ar abundance. Nucl. Instruments Methods Phys. Res. Sect. A: Accel. Spectrometers, Detect. Assoc. Equip. 356, 526–529.

Cerjan, C.J., et al., 2018. Dynamic high energy density plasma environments at the National Ignition Facility for nuclear science research. J. Phys. G: Nucl. Part. Phys. 45, 033003.

Chadwick, M., Herman, M., Obložinský, P., Dunn, M., Danon, Y., Kahler, A., Smith, D., Pritychenko, B., Arbanas, G., Arcilla, R., et al., 2011. ENDF/B-VII.1 nuclear data for science and technology: Cross sections, covariances, fission product yields and decay data. Nucl. Data Sheets 112, 2887–2996.

Collon, P., Bichler, M., Caggiano, J., Cecil, L.D., Masri, Y.E., Golser, R., Jiang, C., Heinz, A., Henderson, D., Kutschera, W., Lehmann, B., Leleux, P., Loosli, H., Pardo, R., Paul, M., Rehm, K., Schlosser, P., Scott, R., Smethie, Jr., W., Vondrasek, R., 2004. Development of an AMS method to study oceanic circulation characteristics using cosmogenic ^{39}Ar. Nucl. Instrum. Methods Phys. Res. B 223–224, 428–434.

Davidenko, V.A., Pogrebov, I.S., Saukov, A.I., 1957. Determination of the excitation function for the reaction T(d, n)He^4. Sov. J. At. Energy 2, 474–476.

Fritz, B., Alexander, T., Johnson, C., Mace, E., Milbrath, B., Hayes, J., 2021. Background concentrations of argon-39 in shallow soil gas. J. Environ. Radioact. 228, 106513.

Goldhagen, P., 2000. Overview of aircraft radiation exposure and recent ER-2 measurements. Health Phys. 79, 526–544.

Goldhagen, P., Clem, J., Wilson, J., 2003. Recent results from measurements of the energy spectrum of cosmic-ray induced neutrons aboard an ER-2 airplane and on the ground. Adv. Space Res. 32, 35–40.

Golovko, V.V., 2023. Application of the most frequent value method for ^{39}Ar half-life determination. Eur. Phys. J. C 83 (930).

Gordon, M., Goldhagen, P., Rodbell, K., Zabel, T., Tang, H., Clem, J., Bailey, P., 2004. Measurement of the flux and energy spectrum of cosmic-ray induced neutrons on the ground. IEEE Trans. Nucl. Sci. 51, 3427–3434.

Gu, J.Q., Tong, A.L., Yang, G.M., Hu, S.M., Jiang, W., Lu, Z.T., Purtschert, R., Ritterbusch, F., 2021. Reconstruction of the atmospheric ^{39}Ar/Ar history. Chem. Geol. 583, 120480.

Hess, W.N., Patterson, H.W., Wallace, R., Chupp, E.L., 1959. Cosmic-ray neutron energy spectrum. Phys. Rev. 116, 445–457.

Hobbs, P.V., 2000. Introduction to Atmospheric Chemistry. Cambridge University Press.

Hou, S., Jenk, T.M., Jiang, W., Zhang, W., Hu, H., Feng, X., Li, H., Wu, S.Y., Pang, H., Yu, J., Huang, R., Lu, Z.T., Yang, G.M., Bender, M., Schwikowski, M., 2025. A radiometric timescale challenges the chronology of the iconic 1992 Guliya ice core. Sci. Adv. 11, eadx8837.

Husain, L., Kuroda, P., 1968. 14.8 MeV neutron activation cross-sections of argon. J. Inorg. Nucl. Chem. 30, 355–359.

Iwamoto, O., Iwamoto, N., Kunieda, S., Minato, F., Nakayama, S., Abe, Y., Tsubakihara, K., Okumura, S., Ishizuka, C., Yoshida, T., et al., 2023. Japanese evaluated nuclear data library version 5: JENDL-5. J. Nucl. Sci. Technol. 60, 1–60.

Klix, A., Döring, T., Domula, A., Zuber, K., 2018. The intensive DT neutron generator of TU Dresden. EPJ Web Conf. 170 (02004).

Koning, A.J., Hilaire, S., Goriely, S., 2023. TALYS: modeling of nuclear reactions. Eur. Phys. J. A 59 (131).

Kostal, M., Czakoj, T., Alexa, P., Šimon, J., Zmeškal, M., Schulc, M., Krechlerová, A., Peltán, T., Mravec, F., Cvachovec, F., Rypar, V., Uhlár, R., Harkut, O., Matěj, Z., 2023. Measurement of dosimetrical cross sections with 14.05 MeV neutrons from compact neutron generator. Ann. Nucl. Energy 191, 109904.

Kutschera, W., Jull, A.J.T., Paul, M., Wallner, A., 2023. Atom counting with accelerator mass spectrometry. Rev. Modern Phys. 95, 035006.

Loosli, H., 1983. A dating method with ^{39}Ar. Earth Planet. Sci. Lett. 63, 51–62.

Loosli, H., Oeschger, H., 1968. Detection of ^{39}Ar in atmospheric argon. Earth Planet. Sci. Lett. 5, 191–198.

MacMullin, S., Boswell, M., Devlin, M., Elliott, S., Fotiades, N., Guiseppe, V., Henning, R., Kawano, T., B.H.LaRoque, R., O'Donnell, J., 2012. Partial γ-ray production cross sections for $(n, xn\gamma)$ reactions in natural argon at 1–30 MeV. Phys. Rev. C 85, 064614.

Mancusi, D., Boudard, A., Cugnon, J., David, J.C., Kaitaniemi, P., Leray, S., 2014. Extension of the Liège intranuclear-cascade model to reactions induced by light nuclei. Phys. Rev. C 90, 054602.

Musy, S., Purtschert, R., 2023. Reviewing ^{39}Ar and ^{37}Ar underground production in shallow depths with implications for groundwater dating. Sci. Total Environ. 884, 163868.

Nassar, H., Paul, M., Ahmad, I., Berkovits, D., Bettan, et al., 2005. Stellar (n, γ) cross section of ^{62}Ni. Phys. Rev. Lett. 94, 092504.

Nobre, G., Brown, D., Arcilla, R., Coles, R., Shu, B., 2024. Progress towards the ENDF/B-VIII.1 release. EPJ Web Conf 294, 04004.

Ozima, M., Podosek, F.A., 2004. Noble Gas Geochemistry, second ed. Cambridge University Press.

Paul, M., Glagola, B.G., Henning, W., Keller, J.G., Kutschera, W., Liu, Z., Rehm, K.E., Schneck, B., Siemssen, R.H., 1989. Heavy ion separation with a gas-filled magnetic spectrograph. Nucl. Instrum. Methods Phys. Res. A 277, 418–430.

Paul, M., Pardo, R.C., Collon, P., Kutschera, W., Rehm, K.E., Scott, R., Vondrasek, R.C., 2019. Positive-ion accelerator mass spectrometry at ATLAS: Peaks and pits. Nucl. Instrum. Methods Phys. Res. Sec. B 456, 222–229.

Riedmann, R.A., Purtschert, R., 2016. Separation of argon from environmental samples for Ar-37 and Ar-39 analyses. Sep. Purif. Technol. 170, 217–223.

Saldanha, R., Back, H.O., Tsang, R.H.M., Alexander, T., Elliott, S.R., Ferrara, S., Mace, E., Overman, C., Zalavadia, M., 2019. Cosmogenic production of ^{39}Ar and ^{37}Ar in argon. Phys. Rev. C 100, 024608.

Silberberg, R., Tsao, C.H., 1973a. Partial cross-sections in high-energy nuclear reactions, and astrophysical applications. I. Targets with Z$\leq$ 28. Astrophys. J. Suppl. 25, 315–333.

Silberberg, R., Tsao, C.H., 1973b. Partial cross-sections in high-energy nuclear reactions, and astrophysical applications. II. Targets heavier than nickel. Astrophys. J. Suppl. 25, 335–367.

Slayman, C., 2011. JEDEC Standards on Measurement and Reporting of Alpha Particle and Terrestrial Cosmic Ray Induced Soft Errors. Springer, US, Boston, MA, pp. 55–76.

Stoenner, R.W., Schaeffer, O.A., Katcoff, S., 1965. Half-Lives of Argon-37, Argon-39, and Argon-42. Sci. 148, 1325.

Tessler, M., Paul, M., Halfon, S., Meyer, B.S., Pardo, R., Purtschert, et al., 2018. Stellar ^{36,38}Ar$(n, \gamma)^{37,39}$Ar reactions and their effect on light neutron-rich nuclide synthesis. Phys. Rev. Lett. 121, 112701.

United States Committee on Extension to the Standard Atmosphere, 1976. U.S. Standard Atmosphere, 1976. NOAA-S/T 76-1562. National Oceanic and Atmospheric Administration, Washington, D.C.

W. Mannhart, D.S., 2007. Measurement of neutron activation cross sections in the energy range from 8 MeV to 15 MeV. PTB-Bericht Bremerhaven, Wirtschaftsverl. NW, Verl. für neue Wiss. N 53.

Woolf, R.S., Sinclair, L.E., Van Brabant, R.A., Harvey, B.J., Phlips, B.F., Hutcheson, A.L., Jackson, E.G., 2019. Measurement of secondary cosmic-ray neutrons near the geomagnetic north pole. J. Environ. Radioact. 198, 189–199.

Xu, J., Calaprice, F., Galbiati, C., Goretti, A., Guray, G., Hohman, T., Holtz, D., Ianni, A., Laubenstein, M., Loer, B., Love, C., Martoff, C., Montanari, D., Mukhopadhyay, S., Nelson, A., Rountree, S., Vogelaar, R., Wright, A., 2015. A study of the trace ^{39}Ar content in argon from deep underground sources. Astropart. Phys. 66, 53–60.

Yokochi, R., Sturchio, N.C., Purtschert, R., 2012. Determination of crustal fluid residence times using nucleogenic ^{39}Ar. Geochim. Cosmochim. Acta 88, 19–26.